The Malkus–Lorenz water wheel revisited

Leslie E. Matson[a)]
Department of Physics, University of Oregon, Eugene, Oregon 97403

(Received 28 February 2006; accepted 16 August 2007)

The Malkus–Lorenz water wheel is analyzed in a more direct way. Two new dimensionless parameters associated with properties of the water wheel are used in place of the traditional Lorenz parameters, which relate only to Lorenz's fluid model. The primary result is a performance map in the new dimensionless parameter space, which shows where the major behavior types occur and associated bifurcations. A slice across this map is examined by a bifurcation plot that shows details of the transitions between various types of behavior. An example of a 12-cup water wheel model is provided, and its behavior is compared over a wide range of parameters on the performance map to that of the Malkus-Lorenz water wheel. It is shown how the map with its water wheel parameters can be simply converted to the map with Lorenz's fluid dynamics parameters. © *2007 American Association of Physics Teachers.*
[DOI: 10.1119/1.2785209]

I. INTRODUCTION

The interest in simple systems having chaotic behavior has continued to grow since Lorenz presented his three-variable set of differential equations over 40 years ago.[1] The work on chaos based on his equations falls into two largely separate approaches. There are studies on the properties of the solutions to the Lorenz equations and a variety of computer simulations[2,3] and working models of the Malkus water wheel. The original water wheel models were developed[4] by Malkus, Howard, and Krishnamurti, who recognized that their idealized mathematical model of the Malkus water wheel obeys a special case of the Lorenz equations.[5] This type of water wheel has leaking cups hanging from its rim, with water entering only the top cup.

Strogatz[6] carefully identified the two components of wheel slowdown and simplified his analysis by correctly treating only their combination. Other formulations[2,5,7] do not include wheel slowdown due to the input water stream. The most detailed analysis[8] includes it, but with an error that cancels the input water drag after the initial transient, although the overall conclusions are affected only for the frictionless wheel case. (Reference 3 has the same error.)

Experimental water wheels are of two types. The simplest one[2,3,7] consists of a few (typically four to twelve) leaky cups hanging from the perimeter of a wheel whose axis may be horizontal or tilted (see Fig. 1). A single stream of water flows into a cup only when one of them is close to the top. A more sophisticated approach,[8] which obeys the Lorenz equations more closely, is to orient the axle so that the wheel is close enough to horizontal so that the fixed cups form a continuous ring with no gaps (see Fig. 2). By providing a series of input water streams, symmetrically placed about the wheel's high point, we can obtain all the same behaviors as with a single stream, significantly reduce the probability of cup overflow, and get the effect of having many more cups than are actually present. In realistic models of nonideal water wheels, cup overflow and various rules for cup leakage and axle friction have been used.[2,3]

The differential equations are developed in Sec. II for an ideal water wheel with a single input water stream at the wheel's high point and with a very large number of cups with no gaps between them. We show that the ideal water wheel equations are equivalent to Lorenz's equations,[1] with his b parameter equal to unity. Section III introduces two dimensionless parameters λ^* and f^* by scaling the distance and time units; these dimensionless parameters are used to determine the performance of a Malkus water wheel. Section IV locates four major bifurcations where the water wheel behavior changes. A behavior map is derived in Sec. V for the ideal Malkus water wheel in λ^*, f^* space showing the major bifurcations, several periodic orbits, and a chaotic example, and presents a bifurcation figure, a slice across the behavior map in which details of bifurcations and performance modes can be seen. Section VI shows the relation between the new water wheel dimensionless parameters and the parameters used in the Lorenz equations. Section VII suggests simple measurements that can be done on an experimental system (its parameters otherwise unknown) for locating a nonideal system on the ideal system's behavior map, and compares the behavior of a nonideal 12-cup computer model to that of the ideal system.

II. MALKUS WATER WHEEL EQUATIONS

Following Malkus[9] and others,[5,6,8] the ideal water wheel characteristics are no cup overflow, cup leakages proportional to the water mass in a cup, and axle friction torque proportional to the wheel speed.

One time constant characterizes the leakage of the cups. Each cup's leakage is proportional to the leakage constant λ times the water mass in the cup. The differential equation and its solution for the kth cup while it has no water input is

$$\frac{dM_k}{dt} = -\lambda M_k \tag{1a}$$

$$M_k(t) = M_k(0)e^{-\lambda t}. \tag{1b}$$

The quantity $1/\lambda$ is the time constant.

The $1/\lambda$ time constant also figures in the initial filling of the cups. The total mass is $M=\Sigma_k M_k$. If the mass rate of the input stream is Q, the differential equation for $M(t)$ and its solution for $M(0)=0$ are

$$\frac{dM}{dt} = Q - \lambda M \tag{2a}$$

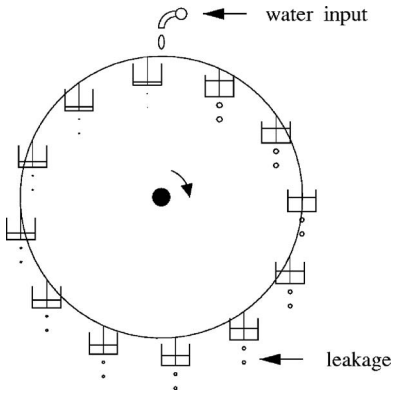

Fig. 1. Twelve-cup water wheel. The wheel's axis is horizontal; water is added at the top, and the hanging cups leak.

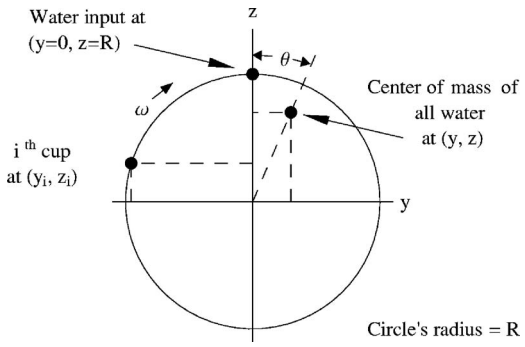

Fig. 3. Water wheel coordinates. The (y,z) coordinate system is in the plane of the wheel, with the cups located on the circle of radius R. A single input stream of water enters the highest cup at the point $(0,R)$. The center of mass of the water in all the cups is located at a point (y,z) within the circle.

$$M(t) = (Q/\lambda)(1 - e^{-\lambda t}). \tag{2b}$$

$M(t)$ starts at zero and approaches the value Q/λ with a time constant of $1/\lambda$, independent of the wheel motion. In the following it is assumed that this initial filling operation has already been finished, so that M is a constant, given by $M = Q/\lambda$.

To derive the equations of motion of the water's center of mass, we split the mass into two parts, and combine what is known about each part to obtain the equations of motion of the overall center of mass. Figure 3 shows the plane of the water wheel with the ring of cups on the circle of radius R. The coordinate system has the y axis horizontal and the z axis in the presumably tilted plane of the water wheel, positive toward the highest point of the wheel, with the origin at the wheel's center. The center of mass of all the water in the cups is at

$$y = \frac{\Sigma\,(M_k y_k)}{\Sigma\,M_k}, \quad z = \frac{\Sigma\,(M_k z_k)}{\Sigma\,M_k}, \tag{3}$$

where the cup with index k contains water mass M_k and is at y_k, z_k.

As shown in Fig. 3 the input water stream continuously enters the top cup at $y=0$ and $z=R$. Select an arbitrary time t_0. For time $t>t_0$ we consider the total water mass to be made up of two components, as if at t_0 the tops of the cups (which continue to leak) are suddenly closed and the input stream of water is then fed into a duplicate set of cups on the wheel, initially empty, but also leaking. The water wheel continues to turn, oblivious to the separation of the water into two groups, because the total water at any point around the wheel is the same as if there were no separation into two groups, one containing the water that entered prior to t_0 and the other with the water added following t_0.

The differential equations for y and z are found by considering the motion of the centers of mass of these two mass sets with masses M_a(t) and M_b(t) respectively. By analogy to Eq. (3),

$$y = \frac{M_a y_a + M_b y_b}{M_a + M_b}, \quad z = \frac{M_a z_a + M_b z_b}{M_a + M_b}, \tag{4}$$

where $t \geq t_0$, and all the quantities are functions of time except for $M_a + M_b = M$, which is a constant. The derivatives of y and z are

$$\frac{dy}{dt} = \frac{1}{M}\left(M_a \frac{dy_a}{dt} + \frac{dM_a}{dt} y_a + M_b \frac{dy_b}{dt} + \frac{dM_b}{dt} y_b\right) \tag{5a}$$

$$\frac{dz}{dt} = \frac{1}{M}\left(M_a \frac{dz_a}{dt} + \frac{dM_a}{dt} z_a + M_b \frac{dz_b}{dt} + \frac{dM_b}{dt} z_b\right). \tag{5b}$$

For $t>t_0$ the M_a cups receive no mass from the input stream. Each cup continues to leak at the rate λM_k and using Eq. (3) it is easy to show that their leakage does not affect the location of their total center of mass. Therefore the center of mass of M_a moves only because of the motion of its cups. Because each cup is fixed on the moving wheel, it follows from a rotation of the coordinates that their center of mass also remains fixed on the wheel and rotates with it. We refer to Fig. 3, replace (y,z) by (y_a,z_a), and define

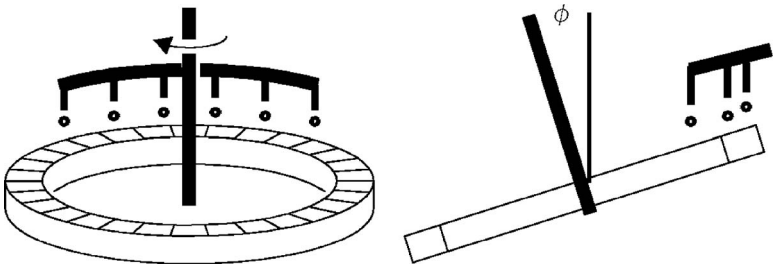

Fig. 2. Continuous-cups water wheel. The axis is tilted so that the fixed cups can form a continuous ring; water enters at several locations, symmetric about the high point.

$$r = \sqrt{y_a^2 + z_a^2}, \quad \theta = \arctan \frac{y_a}{z_a}, \tag{6}$$

where r is constant and $d\theta/dt = \omega$. Thus, the velocity v of the center of mass M_a and its two components can be written as $v = \omega r$ and

$$\frac{dy_a}{dt} = v \cos \theta = \omega z_a \tag{7a}$$

$$\frac{dz_a}{dt} = -v \sin \theta = -\omega y_a. \tag{7b}$$

For the mass M_a at $t = t_0$ we have

$$(M_a = M) \quad \frac{dM_a}{dt} = -\lambda M \tag{8a}$$

$$(y_a = y) \quad \frac{dy_a}{dt} = \omega z \tag{8b}$$

$$(z_a = z) \quad \frac{dz_a}{dt} = -\omega y. \tag{8c}$$

For M_b, its cups are empty at $t = t_0$, but its top bucket at $y = 0$, $z = R$ is beginning to fill, so at $t = t_0$

$$M_b = 0, \quad y_b = 0, \quad z_b = R, \quad \frac{dM_b}{dt} = \lambda M. \tag{9}$$

The quantities dy_b/dt and dz_b/dt are multiplied by zero so will not be needed. The substitution of Eqs. (8) and (9) into Eq. (5) gives the derivatives of the water's overall center of mass location at $t = t_0$:

$$\frac{dy}{dt} = \omega z - \lambda y \tag{10a}$$

$$\frac{dz}{dt} = -\omega y + \lambda (R - z). \tag{10b}$$

The form of Eq. (10) is independent of the choice of t_0 so Eq. (10) is valid for all t and thus is the desired set of differential equations.

The total moment of inertia of the water about the wheel axis is the sum of I_0 for the wheel and I_w for the water:

$$I = I_0 + I_w \tag{11a}$$

$$I_w = \sum_k M_k R^2 = MR^2. \tag{11b}$$

Because M is constant, I is also constant. The rate of change of the angular momentum equals the torque, which is the sum of N_g due to gravity acting on the water's center of mass, N_μ from axle friction, and the torque N_w due to bringing the incoming water stream up to the speed of the cup into which it falls:

$$I \frac{d\omega}{dt} = N_g + N_\mu + N_w. \tag{12}$$

The leaking water exerts no torque on the wheel so does not enter this analysis, although in the alternate analysis used in Refs. 3 and 8, where I is not constant, the angular momentum that is carried off should have been included.

Table I. Water wheel parameters.

Symbol	Meaning
Q	Input water mass rate
λ	Cup leakage parameter
R	Radius where cups are located
I_0	Empty wheel moment of inertia
α	Axle friction parameter
$g \sin \phi$	Gravity in tilted wheel plane
$M = Q/\lambda$	Mass of water
$I_w = MR^2$	Water's moment of inertia
$I = I_0 + I_w$	Total moment of inertia

The torque applied to the wheel by gravity is

$$N_g = Mgy \sin \phi, \tag{13}$$

where g is the gravitational field and ϕ is the tilt angle of the wheel's axis from the vertical, as shown in Fig. 2.

The axle friction torque is proportional to ω and the friction parameter α, and is given by

$$N_\mu = -\alpha\omega. \tag{14}$$

The slowdown torque due to the incoming water stream equals the radius R times the lateral force that brings the stream of water (mass rate $= \lambda M$) up to the cup's lateral speed ωR. In the small time interval Δt a small water mass Δm is deposited, with initial lateral speed equal to zero, so that using I_ω from Eq. (11), we have

$$\text{force} = \frac{(\Delta m) \times (\text{bucket speed-input water speed})}{\Delta t} = (\lambda M)(\omega R - 0) \tag{15}$$

$$N_w = -R \times \text{force} = -\omega \lambda I_w. \tag{16}$$

The substitution of the torques in Eqs. (13), (14), and (16) into Eq. (12) gives

$$\frac{d\omega}{dt} = \frac{Mg \sin \phi}{I} y - \left(\frac{\alpha}{I} + \lambda \frac{I_w}{I} \right) \omega. \tag{17}$$

The parameters of the water wheel are summarized in Table I. We define

$$a = \frac{Mg \sin \phi}{I} \tag{18}$$

$$f = \left(\frac{\alpha}{I} + \lambda \frac{I_w}{I} \right). \tag{19}$$

The differential equations for the water wheel are, after the total mass is stabilized at the value M,

$$\frac{d\omega}{dt} = ay - f\omega \tag{20a}$$

$$\frac{dy}{dt} = \omega z - \lambda y \tag{20b}$$

Table II. Scaling of distance and time units.

Variables	Parameters
$\omega^*=T\omega$	$a^*=DT^2a$
$y^*=y/D$	$f^*=Tf$
$z^*=z/D$	$\lambda^*=T\lambda$
$t^*=t/T$	$R^*=R/D$

$$\frac{dz}{dt}=-\omega y+\lambda(R-z). \tag{20c}$$

In the absence of gravity ($\phi=0$ so $a=0$) Eq. (20a) shows that $1/f$ is the time constant for the slowdown of the wheel due to axle friction and input water drag. Similarly, if $\omega=0$ (the wheel is held stationary), $1/\lambda$ is the time constant for the motion of the water's center of mass toward the water input point at $y=0$ and $z=R$. The coefficient a is the wheel's angular acceleration due to gravity, per unit horizontal displacement of the water's center of mass.

If there are multiple input streams, symmetrically located as in Fig. 2, we denote the radius where the cups and input water streams are located by R_w. We also denote the location of the center of mass of input water deposited in a very short time interval by $y=0$ and $z=R$. All the previous relations still apply, except that the water's moment of inertia I_w in Eqs. (11), (16), (17), and (19), which contributes to the total moment of inertia I, becomes

$$I_w=MR_w^2. \tag{21}$$

III. DIMENSIONLESS PARAMETERS

The system of equations in (20) has four parameters. We are free to choose the distance and time units in which Eq. (20) is expressed. If we change the units by the factors D and T respectively, we obtain the primed variables and parameters shown in Table II. This coordinate transformation method is used to characterize all Malkus water wheels in terms of two dimensionless parameters with direct water wheel meanings.

The parameters D and T can be chosen to satisfy any two conditions of our choice. A useful selection is to set a^* and R^* to unity, achieved by letting $D=R$ and $T=1/\sqrt{Ra}$. We thus replace the four parameter (a, f, λ, and R) set by only two parameters, f^* and λ^*, where

$$f^*=\frac{f}{\sqrt{Ra}},\quad \lambda^*=\frac{\lambda}{\sqrt{Ra}}, \tag{22}$$

with $R^*=1$ and $a^*=1$. The undamped period of the original system, obtained by solving Eq. (20) with $\lambda=f=0$, $z\approx -R$, and y small, is

$$P=\frac{2\pi}{\sqrt{Ra}}. \tag{23}$$

Hence $P^*=2\pi$.

In terms of the two dimensionless parameters f^* and λ^*, Eq. (20) becomes

$$\frac{d\omega}{dt}=y-f^*\omega \tag{24a}$$

$$\frac{dy}{dt}=\omega z-\lambda^* y \tag{24b}$$

$$\frac{dz}{dt}=-\omega y+\lambda^*(1-z), \tag{24c}$$

where ω and the time derivatives are similarly time scaled, and the y and z coordinates are scaled so that the radius of the wheel is unity (asterisks on ω, y, z, and t have been suppressed).

IV. MAJOR BIFURCATIONS

This section, based on material in Refs. 5, 6, and 10, describes how the locations of major bifurcations in (λ^*, f^*) space can be found.

A. The pitchfork bifurcation

The water wheel's stationary points are found by setting the left-hand side of Eq. (24) to zero:

$$0=y-f^*\omega \tag{25a}$$

$$0=\omega z-\lambda^* y \tag{25b}$$

$$0=-\omega y+\lambda^*(1-z). \tag{25c}$$

These equations have three solutions. One is given by

$$z=1,\quad y=0,\quad \omega=0, \tag{26}$$

which is called point C_0 in (ω,y,z) space. (The wheel is stationary, and all the water in the cups is exactly at the top.) The two other solutions are

$$z=\lambda^* f^* \tag{27a}$$

$$y=\pm\sqrt{z(1-z)} \tag{27b}$$

$$\omega=y/f^*. \tag{27c}$$

The latter two points, with real values only when $\lambda^* f^*<1$, are C_1 (negative y and ω) and C_2 (positive y and ω) in (ω,y,z) space, where the wheel speed remains steady in either direction, while the water's center of mass remains fixed in space. When $\lambda^* f^*\geq 1$, the wheel eventually comes to a stop for all initial values of (ω,y,z) at the single stable stationary point C_0.

As $\lambda^* f^*$ passes below unity, the C_1 and C_2 stable stationary points move out from the now unstable C_0, so the system goes from one to three stationary points, hence the pitchfork name. The (ω,y,z) space is therefore now divided into two parts, one in which convergence is to C_1 and the other to C_2. On the boundary between these regions convergence is to the nonstable C_0. This change in the topology of the (ω,y,z) space as $\lambda^* f^*$ passes through unity is called a bifurcation, referred to here as the A bifurcation.[11] In the following, several major bifurcations are identified among the infinite number of bifurcations present of various types.

B. The onset of preturbulence, the B bifurcation

For $f^*=0.2$, as λ^* decreases from $\lambda^*=\lambda_A^*=5$ at the A bifurcation, there are no changes in topology until $\lambda^*=\lambda_B^*\approx 0.1536$, at the B bifurcation.[12] When λ^* becomes less than

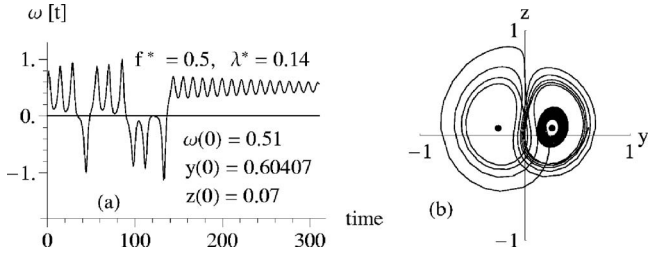

Fig. 4. Example of preturbulence. (a) Plot of the angular velocity versus time. (b) The plot of z versus y shows the path of the center of mass motion in the plane of the wheel. A possibly very long initial period of apparent chaos is followed by convergence to a steady rotation.

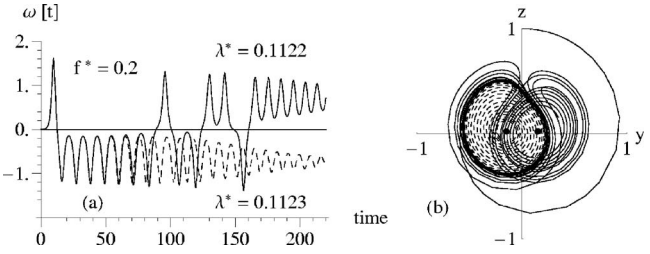

Fig. 6. Bifurcation parameter λ_C^*. Same comments as for Fig. 5, but straddling the λ_C^* point.

λ_B^*, several unstable types of behavior become possible, including periodic orbits, paths that end at C_0, and chaotic paths. Because these are all unstable, the wheel in real experiments will always end up rotating steadily at the C_1 or C_2 stationary points. When the wheel's initial conditions are very close to an unstable chaotic path, the wheel will follow it for a while, reversing direction many times before converging to C_1 or C_2. This behavior is called preturbulence[10] and is illustrated in Fig. 4.

The method for finding the value of λ_B^* involves trials with initial conditions a tiny bit away from the C_0 stationary point (here in the plus ω and y direction, with $z[0]=1$ so that all the water is in the almost stationary top cup). With this starting point, trajectories with $\lambda^* > \lambda_B^*$ converge to C_2, such as the solid trajectory in Fig. 5. A system with $\lambda^* < \lambda_B^*$ gives the dotted trajectory in which the wheel settles instead to C_1. From the z versus y plot it is evident that at λ_B^* the wheel returns to the unstable C_0 starting point, which is called a homoclinic path.[13]

C. The onset of stable chaos: The C bifurcation

For $f^*=0.2$, as λ^* becomes less than λ_B^*, there are no bifurcations until $\lambda^*=\lambda_C^* \approx 0.1123$. The C bifurcation[14] is the leading edge of a host of minor bifurcations; two of its properties are identified here. The first is that for $\lambda^* < \lambda_C^*$ chaotic paths become stable. The second property provides a method that we will use to locate λ_C^*.

If we start from the initial conditions used for locating λ_B^*, for all values of λ^* between λ_B^* and λ_C^* the trajectory will be similar[10] to the dotted curve in Fig. 5. The dotted curve in Fig. 6 is for λ^* slightly larger than λ_C^*, so it is similar to the dotted curve in Fig. 5. The closer λ^* is to λ_C^*, the longer the wheel stays near an unstable periodic orbit and loops about C_1 before it converges to C_1 with its constant counterclockwise wheel rotation. When λ^* is slightly less than λ_C^*, as shown by the solid curve in Fig. 6, the path eventually leaves the periodic orbit, the wheel reverses direction at least once, and ends at either C_1 or C_2. When λ^* exactly equals λ_C^* the trajectory must converge to the unstable orbit from which the above C and below C trajectories eventually diverge. Such a trajectory is called a heteroclinic path.[15]

Because the chaotic paths are stable below λ_C^*, they are surrounded by a basin of attraction. A trajectory started within such a basin will follow a chaotic path forever (see Fig. 7). Below λ_C^* there also can be basins of attraction where the trajectories approach stable periodic orbits, and paths that converge to C_1 or C_2.

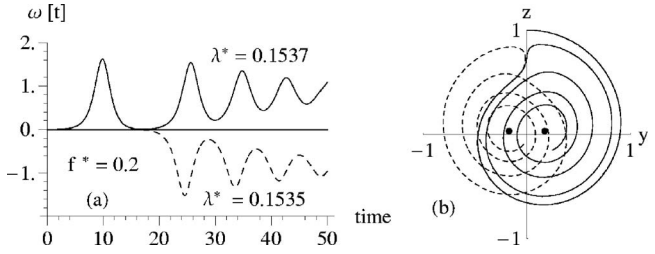

Fig. 5. Bifurcation parameter λ_B^*. Plots of (a) angular velocity versus time and (b) the center of mass motion are shown for a pair of values of λ^* that straddle the value of λ_B^*. The initial conditions are very close to the C_0 stationary point at $\omega=y=0$, and $z=1$.

D. The Hopf bifurcation

As λ^* is reduced below λ_C^*, the unstable periodic orbit involved in the C bifurcation contracts onto C_1, and its mirror onto the C_2 point. When these unstable orbits disappear by combining with the stationary points, the two stationary points become unstable. This behavior is called a Hopf bifurcation[6] and occurs at $\lambda_D^* \approx 0.0889$, where $f^*=0.2$ in the relation[16]

$$\lambda_{\text{Hopf}}^* = \frac{f^*}{2}\left(\frac{1-f^{*2}}{1+2f^{*2}}\right). \tag{28}$$

When λ^* is less than λ_D^*, where the C_1 and C_2 stationary points are unstable, three types of stable behavior are identified: (a) paths that loop about but eventually converge onto an exactly repeating periodic orbit that can have one or many loops about C_1 and C_2; (b) paths that stay near a repeating orbit but never converge to it ("noisy periodicity"); or (c) chaos, where the wheel reverses direction randomly, the path switching between loops about C_1 and C_2.

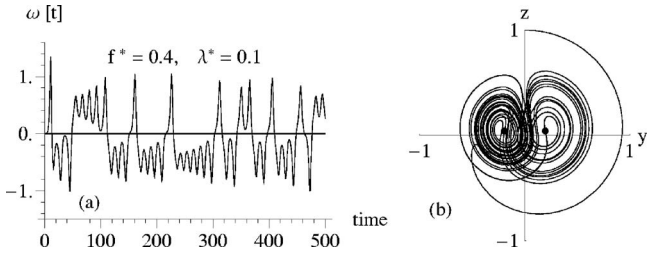

Fig. 7. Example of a chaotic orbit.

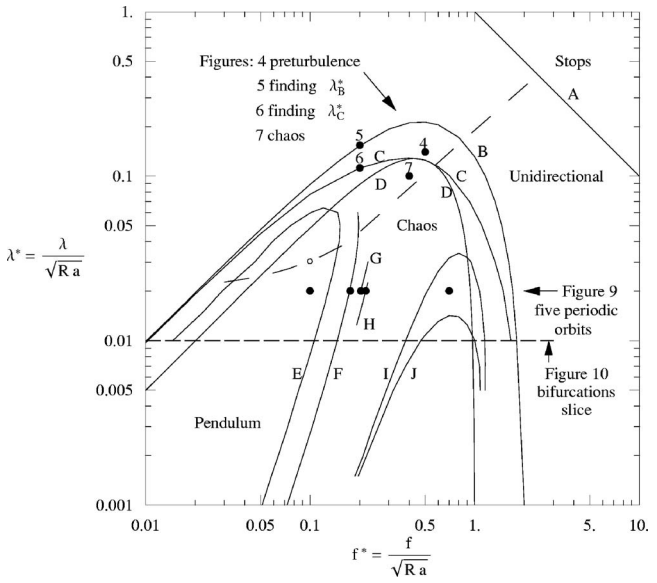

Fig. 8. Water wheel map for the water wheel parameters (λ^*, f^*). Above the A curve the wheel always comes to a stop. Between the A and C bifurcation curves the only stable behavior is steady unidirectional motion. Between the C and D curves, steady turning, periodic motion, or chaos results depending on the initial conditions. Below the D curve there are only periodic orbits or chaos. Periodic orbit examples are symmetric pendulum motion within the E contour, a "fill and fall" motion between I and J, and others in an infinite number of narrow strips such as the partial curves F, G, and H, which lie in the chaotic region. The horizontal dashed line shows where the bifurcation plot of Fig. 10 is located, with only α changing. The curved dashed line is an example with only the input water rate Q changing.

V. THE WATER WHEEL BEHAVIOR MAP

Figure 8 is a map indicating the behavior of the Malkus water wheel. The A, B, C, and D bifurcations are shown as completed contours, extended to other values of f^*, thus bounding the regions for the various behavior that we have noted. The locations of the parameters producing Figs. 4–7 are indicated by dots. The horizontal dashed line is an example where only the axle friction α is changed. The curved dashed line is an example where only the input water rate Q changes, with $Q=0.0001$ at the upper right, 0.0307 at the circle, and 10.0 at the lower left. For infinite Q the curve would end at $\lambda^*=f^*=0.02182$, approximately on the B curve. The fixed parameters for this curve are $R=0.25$, $I_0=0.025$, $\phi=15°$, $\alpha=0.01$, and $\lambda=0.0695$.

A. Periodic orbit examples

Figure 8 also has five dots along $\lambda^*=0.02$ that locate the parameters for the five periodic orbits shown in Fig. 9. Figure 9(a) shows the initial path of the water's center of mass for the pendulum case, starting with all the water at almost the top of the wheel. The plots in Figs. 9(b)–9(f) show enlarged plots of the final stable orbits. The symmetric pendulum orbit (b) is found everywhere within the E curve. Bordering the E curve are nonsymmetric pendulum versions, and similar orbits that repeat only after completing more than one cycle, called period-doubled orbits. As always, other initial conditions can lie in other basins of attraction, leading to other behavior.

The curves F, G, and H in Fig. 8 locate portions of the regions, some extremely narrow, where the "pumpkin," "one-two," and "happy face" orbits of Fig. 9 can be found. In the pendulum case in Fig. 9(b), the orbit loops about C_1, then C_2, and repeats. In the pumpkin case Fig. 9(c), the orbit makes two loops about C_1, two loops about C_2, and repeats. For the nonsymmetric one-two case in Fig. 9(d), the orbit loops once about C_1 and then twice about C_2. The happy face in Fig. 9(e) has three loops about C_1 and then three about C_2. The looping is in three dimensions, so that some loops are not well shown in the (y,z) projection.

Between the I and J contours the trajectory converges to a stable symmetric orbit in which the top bucket fills until the wheel, slightly off balance, falls to the left or the right on alternate cycles, almost stops due to axle friction, only to fill the new top bucket, as in the "fill and fall" case shown in Fig. 9(f).

B. Bifurcation diagrams

The spiderlike Fig. 10 shows a cross section of the Fig. 8 map along the $\lambda^*=0.01$ line, showing bifurcations where the behavior changes. At the left and right edges of Fig. 10 are single lines where unidirectional motion occurs, with some switching between the two directions of motion, resulting in dotted lines. The symmetric pendulum with six extrema as in Fig. 9(b) occurs between the two E markers. At the E bifurcation where $f^*\approx 0.11$, the trajectory switches from a symmetric pendulum to an asymmetric pendulum motion, then proceeds (difficult to see in Fig. 10) through period-doubling and noisy periodicity into chaos. At most values of f^* in the chaotic region, $0.13<f^*<0.3$, the dots for the y extrema (see Fig. 7) overlap to draw a continuous line, with spaces between outliers that would be filled in if the run length were increased. There are an infinite number of gaps in the chaotic region where stable orbits occur, such as the pumpkin at F, but most are extremely narrow so cannot be seen. The symmetric orbit in Fig. 9(f) is seen in Fig. 10 within the I-to-J and J-to-I regions. Between the two J labels for $0.64<f^*<0.86$ lie a pair of asymmetric orbits,[17] each consisting of one side of the fill and fall case. Due to switching between the two orbits as f^* is varied, the two lines for each orbit are

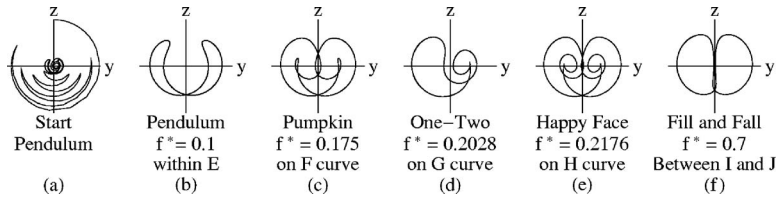

Fig. 9. Examples of stable periodic orbits. The motion of the water's center of mass in the plane of the wheel is shown for five stable orbits, all with $\lambda^*=0.02$, located at five dots on Fig. 8. (a) Plot of the initial transient behavior leading to the periodic pendulum stable orbit. The final pendulum orbit and the other final orbits are shown enlarged in (b)–(f). The starting points are all close to C_0.

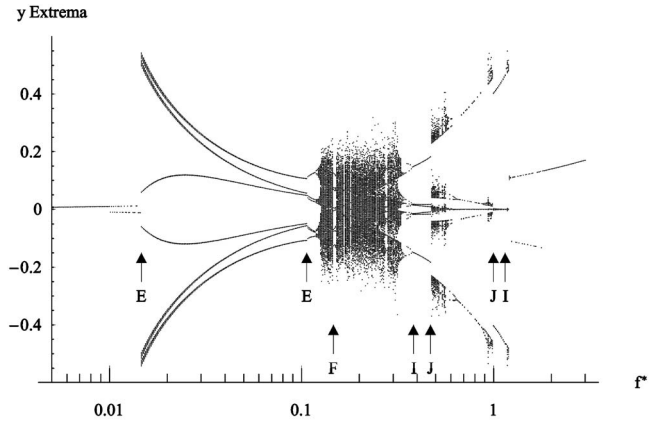

Fig. 10. Bifurcation diagram for $\lambda^*=0.01$ (see dotted line in Fig. 8). For each value of f^* from 0.005 through 3.0 a run was started close to C_0 as was done for Fig. 8 and run for 4000 s for the initial transient to be removed. For the next 4000 s a dot is placed in the figure at each extremum (change in direction) of the y coordinate of the center of mass. Abrupt changes as f^* is varied indicate bifurcations.

dotted, indicating bifurcations or floating point error. From the J label at $f^*=0.48$ to about $f^*=0.56$ lies an extended region of noisy periodicity.

VI. RELATION TO THE LORENZ EQUATIONS AND PARAMETERS

In this section we relate the parameters λ^* and f^*, which are convenient for describing the water wheel, to the Lorenz parameters σ, r, and b. A standard form of Lorenz's equations[5] is

$$\frac{dx}{dt}=\sigma y-\sigma x \tag{29a}$$

$$\frac{dy}{dt}=x(r-z)-y \tag{29b}$$

$$\frac{dz}{dt}=xy-bz. \tag{29c}$$

These equations represent the convection of a restricted region of fluid with heat applied at the bottom, $y=z=0$ (corresponding to water added to the top of a water wheel), and fluid rotation at the rate x about the point $y=0$, $z=r$.

If we make the substitutions $z\rightarrow r-z$ and $x\rightarrow\omega$, we find an alternative form where the fluid is cooled at the top. This form is similar to Eq. (20):

$$\frac{d\omega}{dt}=\sigma y-\sigma\omega \tag{30a}$$

$$\frac{dy}{dt}=\omega z-y \tag{30b}$$

$$\frac{dz}{dt}=-\omega y+b(r-z). \tag{30c}$$

We use the coordinate rescaling in Table II and relate Eq. (20) to Eq. (30) as follows. Start from the general water wheel equation, Eq. (20), and apply the change of variables in Table II. We then solve for the scaling factors T and D by requiring $a^*=f^*$ to satisfy Eq. (30a) and require $\lambda^*=1$ to satisfy Eq. (30b). The result is $T=1/\lambda$ and $D=\lambda f/a$, which (dropping the asterisks on ω, y, z, and t) transforms Eq. (20) to

$$\frac{d\omega}{dt}=\frac{f}{\lambda}y-\frac{f}{\lambda}\omega \tag{31a}$$

$$\frac{dy}{dt}=\omega z-y \tag{31b}$$

$$\frac{dz}{dt}=-\omega y+\left(\frac{Ra}{f\lambda}-z\right). \tag{31c}$$

After substituting the expressions for f and λ from Eq. (22) into Eq. (31), a comparison with Eq. (30) shows that the f^* and λ^* parameters are related to the Lorenz parameters by

$$\sigma=\frac{f^*}{\lambda^*} \tag{32a}$$

$$r=\frac{1}{f^*\lambda^*} \tag{32b}$$

$$b=1, \tag{32c}$$

or

$$f^*=\sqrt{\frac{\sigma}{r}} \tag{33a}$$

$$\lambda^*=\frac{1}{\sqrt{\sigma r}}. \tag{33b}$$

The upper and right borders of Fig. 11 indicate how the above relations lead to a simple conversion of the water wheel maps from (f^*,λ^*) coordinates to the conventional Lorenz coordinates.

VII. SUGGESTIONS FOR EXPERIMENTS

A. Finding values of the parameters for a nonideal system

An actual water wheel will deviate from the ideal system characteristics specified in Sec. II, because, for example, the water will be in discrete cups that overflow, and the leakage rate will not be proportional to the water mass in a cup. A way is needed to determine the approximate values of λ^* and f^* for the water wheel. The method chosen here ignores the complexity of multicup systems for simplicity. Its advantage is that it requires no prior data about the system, so it is particularly convenient for real systems.

Starting from the given initial conditions, let the water wheel run until its initial transient behavior has finished. Then, as the wheel continues to run, collect the leakage and cup overflow water (not including the water that misses the cups) in a time interval, and calculate the average total leakage-plus-overflow water mass rate Q_{eff}. The latter equals the effective input water rate, which is different from the input spigot's rate because some of the water misses the cups. Next, quickly shut off the water and measure the mass M of all the water in the cups. Do this measurement several

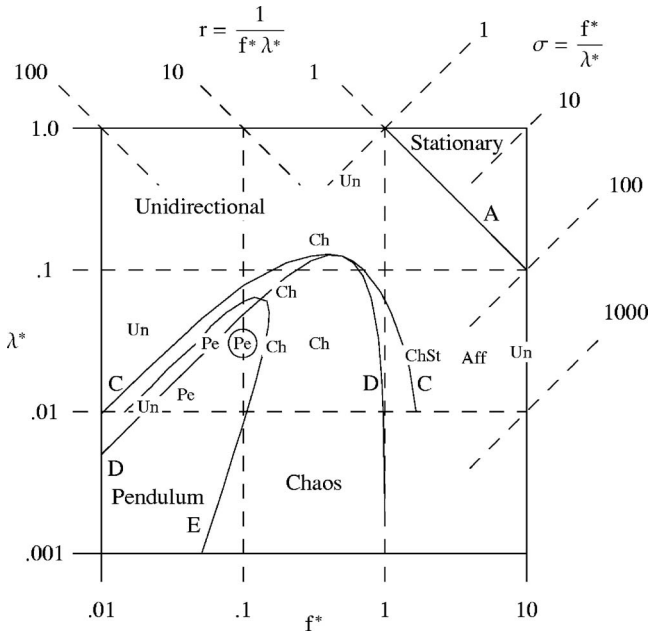

Fig. 11. (a) The top and right borders indicate the standard Lorenz parameters (σ, r, with $b=1$) for this plot and for Fig. 8. (b) As in Fig. 8, λ^* and f^* are proportional to the inverse of the cup leakage and wheel slowdown time constants, respectively. The A, C, D, and E contours are for the ideal Malkus–Lorenz wheel, for which steady unidirectional motion occurs only between curves A and D, chaos is found only below curve C, and symmetrical pendulum motion occurs only within curve E. The labels Un, Pe, Ch, ChSt, and Aff indicate the type of motions (Unidirectional, Pendulum, Chaos, Chaos-then-Stationary, and Asymmetric fill-and-fall) found for a computer model of a 12-cup wheel, at the corresponding locations on this simplified version of Fig. 8. The (f^*,λ^*) values were found using the procedure outlined in Sec. VII A. The behavior of the 12-cup wheel is generally similar to that of the ideal water wheel, except for large f^*.

times to obtain averages for Q_{eff} and M. From Eq. (1a) the average leakage time constant $1/\lambda$ equals M/Q_{eff}. Note that for the ideal system $1/\lambda$ is constant, independent of the wheel's action, while for a nonideal system it depends on the changing water distribution among the cups. Hence we are estimating an average value (sometimes a very rough estimate).

Next, with no water input, attach a mass M (as measured in the previous paragraph) to a bottom cup, displace the wheel by a small angle, and measure the period P of the pendulum-type motion [see Eq. (23)]. The axle friction should be made small enough to see periodic motion.

Two more measurements are needed to find the wheel slowdown time constant $1/f$. As in Eq. (19), it depends on α/I, λ, and I_w/I. The ratio I/α is the wheel slowdown time constant when the cups all have equal masses totaling M. To measure it attach two masses $M/2$ to opposite cups with no water input, so that gravity and the input stream drag have no effect, and start the wheel at a typical speed. The quantity I/α is the total angle traveled divided by the initial angular rate.

The ratio I_w/I is found using I/α and the empty time constant τ_0. The latter can be found by the same procedure, but with the two $M/2$ masses removed, or placed exactly at the wheel's center to keep the load on the axle the same. The time constant τ_0 is less than I/α because removing the masses reduces the moment of inertia. Because the moments of inertia are proportional to the corresponding time constants, and $I_w=I-I_0$, we have

$$\frac{I_w}{I}=\left(1-\frac{\tau_0}{I/\alpha}\right). \tag{34}$$

The substitution of the values obtained for I_w/I, α/I, and λ into Eq. (19) gives the value of f. Finally, using Eqs. (22) and (23), the values of λ^* and f^* are found from

$$\lambda^*=\lambda\frac{P}{2\pi},\quad f^*=f\frac{P}{2\pi}. \tag{35}$$

Table III. Variables and parameters for the 12-cup water wheel. SI units are used.

Symbol	Meaning
θ	Angle of rotation of wheel
ω	Angular velocity of wheel
M_k	Mass of water in kth cup
$M_0=0.4$	Cup overflows above this mass
$R=0.25$	Radius of wheel
$I_0=0.025$	Moment of inertia of wheel without water
$\phi=15°$	Wheel axis tilt from vertical
$L=0.0146$	Cup leakage parameter
Q	Total water flowing from spigot
α	Axle torque/axle speed

B. Computer model of a nonideal water wheel

To illustrate the use of the water wheel map in Fig. 8, a 12-cup computer model was set up using MATHEMATICA. The same procedures as in Sec. VII A can be used to determine average values for Q_{eff}, M, and then P, I/α, and I_w/I and used to locate a nonideal system on the water wheel map, shown with less detail in Fig. 11. The variables and parameters are given in Table III. If we use the cup model in Ref. 3, the water rate actually received by the kth cup is the following function of θ_k, which approximates a contoured input stream as wide as a cup:

$$Q_k=Q\cos^{1000}\theta_k/2, \tag{36}$$

where $\theta_k=\theta+k2\pi/12$, and the exponent 1000 gives a cup width of $\approx 4.2°$. Overflow is modeled by an exponential function, with overflow equal to leakage at $M_k=M_0$. If we include the moment of inertia I_0 of the wheel itself, the equations of the system are

$$\frac{dM_k}{dt}=Q\cos^{1000}\theta_k/2-L\sqrt{M_k}-L\sqrt{M_0}\exp\left(\frac{M_k-M_0}{M_0/20}\right) \tag{37a}$$

$$\frac{d\omega}{dt}\left(I_0+\sum_{k=1}^{12}R^2M_k\right)+\omega\sum_{k=1}^{12}R^2Q\cos^{1000}\theta_k/2$$
$$=R\sin\phi\sum_{k=1}^{12}M_kg\sin\theta_k-\alpha\omega, \tag{37b}$$

with $d\theta/dt=\omega$. Because water leakage and overflow exert no torque on the wheel, they do not enter Eq. (37b).

C. Performance examples

Figure 11 is the water wheel map showing the location of a number of system points (λ^* and f^*) for examples of the 12-cup computer model as the water input rate Q and the axis friction coefficient α are varied. The notations Un, Pe, Ch, ChSt, and Aff indicate the system's motion type, as Unidirectional, Pendulum, Chaos, Chaos-then-Stationary, and Asymmetric fill-and-fall, respectively. All initial conditions are close to C_0. The system at the circled Pe has $Q=0.1$ and $\alpha=0.01$, equivalent to that for the circle in Fig. 8. Extending from left to right from the circled Pe, the values for α vary from zero to 1.2. Another sequence of points from lower left to upper right, also including the circled Pe, have Q varying from 0.5 to 0.02.

The behaviors generally agree with those of the ideal Malkus water wheel, which are bounded by the A, C, D, and E curves in Fig. 11, except for large α and f^*, where axle friction often causes the wheel to stop completely between cups, as in the ChSt example. For the Aff example the behavior is similar to that of the ideal system in $0.65<f^*<0.85$ in Fig. 10, but the f^* value of 4.3 is well outside that range.

VIII. SUMMARY

We have shown that the ideal water wheel devised by Malkus can be characterized by two dimensionless parameters λ^* and f^*, which are identified with the inverses of the time constants for cup leakage and wheel slowdown. These two water wheel parameters are shown to be simply related to Lorenz's fluid dynamics parameters. The water wheel behavior map in (λ^*, f^*) space shows where the major behavior types are separated by bifurcation curves, and the methods to locate the curves are illustrated. The map shows where chaotic behavior and several examples of periodic orbits are found. A transverse slice across this map is shown in a bifurcation plot. The positioning of this bifurcation slice, which differs from those in Refs. 5 and 8 has the advantage of probing a wide variety of behaviors.

A computer model of a nonideal 12-cup water wheel was used to illustrate the usefulness and limitations of the ideal water wheel map in predicting and understanding the performance of actual water wheels that exhibit chaos.

ACKNOWLEDGMENTS

The work was initiated following suggestions by Professor Robert L. Zimmerman, University of Oregon, who provided essential guidance. Consultations with Professor Godfrey Gumbs, Hunter College, are greatly appreciated, as is assistance in the required file format conversions by Rakesh Venkatesh, Tufts University. Many excellent suggestions by the unknown reviewers were gratefully incorporated.

[a]Electronic mail: matson@rosenet.net

[1]Edward N. Lorenz, "Deterministic non-periodic flows," J. Atmos. Sci. **20**, 130–141 (1963).

[2]J. Louis Tylee, "Chaos in a real system," Simulation **64**(3), 176–183 (1995).

[3]Aaron Clauset, Nicky Grigg, May Lim, and Erin Miller, www.santafe.edu/~aaronc/ClauGrigLimMill_SFI03_ChaosYouCanPlayIn.pdf

[4]Edward N. Lorenz, *The Essence of Chaos* (University of Washington Press, Seattle, WA, 1993), p. 143.

[5]Colin Sparrow, *The Lorenz Equations: Bifurcations, Chaos, and Strange Attractors* (Springer-Verlag, New York, 1982), Chapter 1 and Appendix B.

[6]Steven H. Strogatz, *Nonlinear Dynamics and Chaos* (Perseus Books, Cambridge, MA, 1994).

[7]Fritz Gassmann, "Noise-induced chaos-order transitions," Phys. Rev. E **55**, 2215–2221 (1997).

[8]Miroslav Kolář and Godfrey Gumbs, "Theory for the experimental observation of chaos in a rotating waterwheel," Phys. Rev. A **45**, 626–637 (1992).

[9]Willem V. R. Malkus, "Non-periodic convection at high and low Prandtl number," Mem. Soc. R. Sci. Liege Collect. **IV**, 125–128 (1972).

[10]James L. Kaplan and James A. Yorke, "Preturbulence: A regime observed in a fluid flow model of Lorenz," Commun. Math. Phys. **67**, 93–108 (1979).

[11]The A bifurcation is at $r=1$ in Ref. 5.

[12]The B bifurcation is at r' in Ref. 5.

[13]See Ref. 6, p. 161.

[14]The C bifurcation is at r_A in Ref. 5.

[15]See Ref. 6, p. 166.

[16]The D bifurcation is at r_H in Ref. 5, pp. 10 and 11, converted using Eq. (32).

[17]These are the simplest stable periodic orbits, first reported in Ref. 8.